Peer-reviewed version available at *Int. J. Mol. Sci.* **2018**, *19*, 2149; doi:10.3390/ijms19082149

Tailored biodegradable and electroactive poly(hydroxybutyrate-co-hydroxyvalerate) based morphologies for tissue engineering applications

Luís Amaro[1], Daniela M. Correia[2,3], Teresa Marques-Almeida[1], Pedro M. Martins[1,4], Leyre Pérez[3,5], José L. Vilas[3,5], Gabriela Botelho[4], Senentxu Lanceros-Mendez[3,6], Clarisse Ribeiro[1,7]

[1] Centro/Departamento de Física, Universidade do Minho, 4710-057 Braga, Portugal; cribeiro@fisica.uminho.pt (C.R.)
[2] Departamento de Química e CQ-VR, Universidade de Trás-os-Montes e Alto Douro, 5001-801 Vila Real, Portugal; dcorreia@utad.pt
[3] BCMaterials, Basque Center for Materials, Applications and Nanostructures, UPV/EHU Science Park, 48940 Leioa, Spain; senentxu.lanceros@bcmaterials.net
[4] Centro/Departamento de Química, Universidade do Minho, 4710-057 Braga, Portugal; gbotelho@quimica.uminho.pt
[5] Macromolecular Chemistry Research Group (labquimac), Department of Physical Chemistry, Faculty of Science and Technology, University of the Basque Country (UPV/EHU), Spain
[6] IKERBASQUE, Basque Foundation for Science, 48013 Bilbao, Spain
[7] CEB - Centre of Biological Engineering, University of Minho, 4710-057 Braga, Portugal

* Correspondence: senentxu.lanceros@bcmaterials.net;

Abstract

Polymer-based piezoelectric biomaterials have already proven their relevance for tissue engineering applications. Further, the morphology of the scaffolds plays also an important role in cell proliferation and differentiation. The present work reports on poly(hydroxybutyrate-co-hydroxyvalerate) (PHBV), a biocompatible, biodegradable and piezoelectric biopolymer that has been processed in different morphologies, including films, fibres, microspheres and 3D scaffolds. Further, the corresponding magnetically active PHBV-based composites were also produced. The effect of the morphology on physico-chemical, thermal, magnetic and mechanical properties of pristine and composites samples was evaluated, as well as their cytotoxicity. It was observed that the morphology does not strongly affect the properties of the pristine samples but the introduction of cobalt ferrites induces changes in the degree of crystallinity that could affect the applicability of prepared biomaterials. Young modulus is dependent of the morphology and also increases with the addition of cobalt ferrites. Both, pristine and PHBV/cobalt ferrite composite samples are no cytotoxic, indicating their suitability for tissue engineering applications.

Keywords: biomaterials; cobalt ferrites; poly(hydroxybutyrate-co-hydroxyvalerate); tissue engineering

Peer-reviewed version available at Int. J. Mol. Sci. 2018, 19, 2149; doi:10.3390/ijms19082149

1. Introduction

Tissue engineering aims to restore lost or damaged tissues or organs [1]. With this purpose, the most common approach is the use of scaffolds capable of providing structural support for cells to attach and differentiate into specific tissues [1-2]. Following a biomimetic approach, these scaffolds must also provide biophysical stimuli emulating the native properties of the extracellular matrix (ECM) and hence enhancing cell differentiation [1,3].

The design of the scaffold is a complex process since it must accomplish several requirements, namely biocompatible to avoid inflammatory responses and biodegradable so it will gradually give place to new tissues [4-5]. The scaffold morphology is an important parameter since it should mimic the structure of the native ECM, promoting differentiation into specific cell lines [1-2]. Thus, it must be tailored according to the application [3]. Tailored mechanical properties are also important for the scaffold does not break during handling [4] and to mimic cell natural environment. Therefore, the choice of the used material is the key factor to success. Some smart materials like poly-L-lactic acid (PLLA) [6], polyvinylidene fluoride (PVDF) [7], polyhydroxybutyrate (PHB) [8] and polyhydroxybutyrate-co-hydroxyvalerate (PHBV) [9] have been successfully used to produce scaffolds. PVDF, PLLA, PHB, and PHBV are piezoelectric, producing local electric potentials upon mechanical stimulation [10-12]. Many tissues in the human body show this property, such as skin, bone, muscle, and tendon, thus, smart materials can also provide this stimulus capable of enhancing tissue differentiation [13-14]. The application of smart materials enables the production of such stimuli without the need of wires and power supplies, being the mechano-electrical stimuli produced during motion [15].

Among the different electroactive polymers, PHBV is of increasing interest. It is a co-polymer of PHB from the polyhydroxyalkanoates (PHA) family, and shows large potential for tissue engineering, due to its biocompatibility, bioactivity and piezoelectric properties. It shows better mechanical properties than PHB, and is biodegradable [4,16], which represents an advantage with respect to PVDF, the most used piezoelectric polymer for tissue engineering applications in different morphologies [15,17].

In some applications, specific smart materials alone do not have all the needed/desired properties for tissue regeneration, and polymer composites must be developed. In this way, the combination of magnetostrictive nanoparticles and piezoelectric polymers

Preprints (www.preprints.org) | NOT PEER-REVIEWED | Posted: 3 July 2018 doi:10.20944/preprints201807.0021.v1

Peer-reviewed version available at Int. J. Mol. Sci. 2018, 19, 2149; doi:10.3390/ijms19082149

offers the possibility of developing magnetoelectric materials [18], that, together with magnetic bioreactors allows the generation of local potentials on the scaffolds, which can be advantageous for mimicking specific environments and stimulate specific tissues regeneration [17-18]. These materials have the ability to convert magnetic stimuli in electrical one [19], producing local electric potentials upon magnetic stimulation [20]. Magnetoelectric materials have shown its relevance in neural [21], bone [18,22] and muscle [22] engineering.

In this work, magnetoelectric biodegradable and biocompatible composites are produced. The magnetoelectric composite was developed combining cobalt ferrite particles (CFO) on a PHBV matrix. These particulate composites show important advantages for applications when compared to other magetoelectric composites, such as laminates [23-24] and allow the preparation of porous scaffolds, fibres, films and spheres. This work demonstrates that both PHBV and the magnetoactive composite PHBV + CFO can be processed in the most common structures for tissue engineering applications without changing the main physico-chemical characteristics of the polymer and maintaining its biocompability.

2. Experimental section

2.1. Materials

Poly(hydroxybutyrate-co-hydroxyvalerate), PHBV, (M_w=460,64 g.mol^{-1}; HV=3%, mole fraction), 99% purity, was supplied from *Natureplast* and polyvinyl alcohol (PVA) (M_w=13 – 23 g.mol^{-1}), 98% purity, from Sigma-Aldrich. Cobalt ferrite, CFO, nanoparticles with 35-55 nm particle size were purchased from Nanoamor. Chloroform, 99% purity, and sodium chloride (NaCl), 99% purity, were purchased from Fischer. All materials were used as received from the provider.

It is to notice that the CFO filler content has been selected as 10% wt in order to provide proper magnetic and magnetoelectric response as in analogous systems [25-26] without hindering the mechanical properties and stability of the structure [27].

Preprints (www.preprints.org) | NOT PEER-REVIEWED | Posted: 3 July 2018 doi:10.20944/preprints201807.0021.v1

Peer-reviewed version available at Int. J. Mol. Sci. 2018, 19, 2149; doi:10.3390/ijms19082149

2.2. Preparation of the polymer solution

PHBV was dissolved in chloroform to achieve a polymer concentration of 10% (w/v). The solution was prepared under constant magnetic stirring at 40 ºC until complete dissolution of the polymer. Magnetic composites were also prepared by the method above described: after the dispersion of 10% (w/w) of the CFO nanoparticles in the chloroform solution into an ultrasound bath during 1.5 h, to ensure good dispersion of the CFO nanoparticles and avoid nanoparticles agglomeration, the PHBV optimized concentration of 10% (w/v) was added and magnetically stirred to complete polymer dissolution.

These polymer solutions were used to process the PHBV into different morphologies: films, fibres and scaffolds.

2.3. Processing of PHBV into different morphologies

2.3.1. Films

PHBV and PHBV/CFO composite films were obtained by the solvent casting method. After complete polymer dissolution, the samples were produced by spreading the solution on a clean glass substrate and solvent evaporation at room temperature (Figure 1).

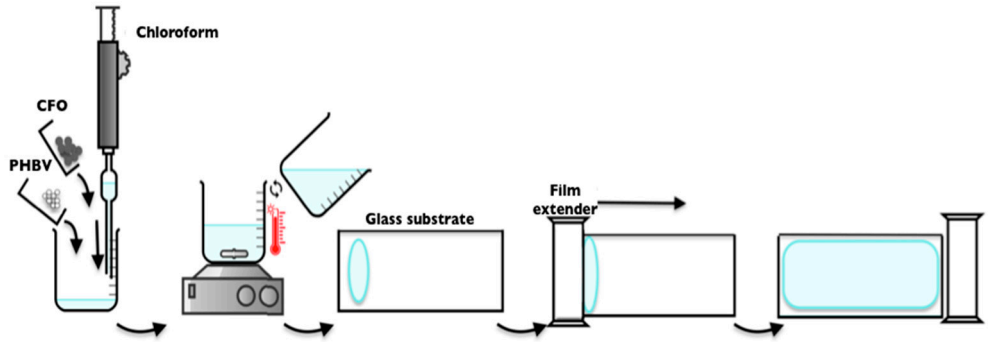

Figure 1 - Schematic representation of the processing of the PHBV films by solvent casting.

2.3.2. Electrospun fibres

Neat and composite PHBV fibres were obtained by electrospinning (Figure 2). The polymer solution was placed in a plastic syringe (10 mL) fitted with a steel needle with an inner diameter of 0.5 mm. The electrospinning process was conducted by applying a

Preprints (www.preprints.org) | NOT PEER-REVIEWED | Posted: 3 July 2018 doi:10.20944/preprints201807.0021.v1

Peer-reviewed version available at Int. J. Mol. Sci. 2018, 19, 2149; doi:10.3390/ijms19082149

voltage of 20 kV with a PS/FC30P04 power source from Glassman with a solution feed rate of 1 $mL.h^{-1}$. Random and aligned fibres were collected using a grounded collecting plate or a rotating collector, respectively, placed at 15 cm from the needle tip.

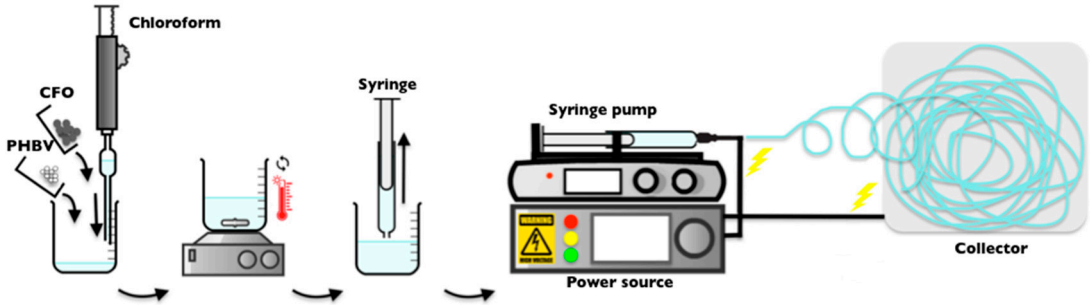

Figure 2 - Schematic representation of the processing of the electrospun fibres.

2.3.3. Microspheres

Neat and magnetic PHBV microspheres were produced, according with the method previously reported, after minor modifications [26] by an oil-in-water emulsion method (Figure 3). After complete polymer dissolution 3% (w/v) in chloroform at 40 ºC, the mixture was added to 0.5% (w/v) of PVA solution in a ratio of 1:10. The emulsified suspension was mechanically stirred at 1000 rpm during 24 h at room temperature, occurring at the same time, the evaporation of the chloroform. The resulting microspheres were washed with ultra-pure water and let dry at room temperature.

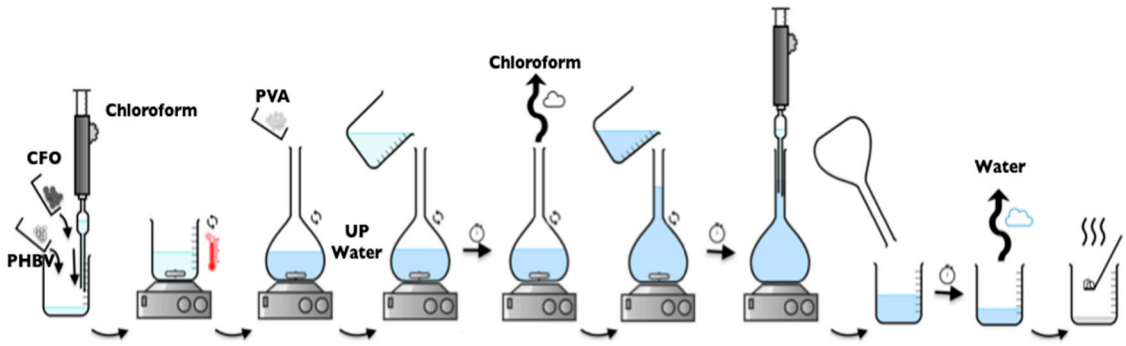

Figure 3 - Schematic representation of the oil-in-water emulsion method for the preparation of microspheres.

2.3.4. Scaffolds

PHBV and PHBV composite scaffolds were produced using the solvent casting via particulate leaching method [2]. The polymer solution was added in a petri dish

Preprints (www.preprints.org) | NOT PEER-REVIEWED | Posted: 3 July 2018 doi:10.20944/preprints201807.0021.v1

Peer-reviewed version available at Int. J. Mol. Sci. 2018, 19, 2149; doi:10.3390/ijms19082149

containing 10 g of NaCl and mixed to obtain a homogeneous dispersion. The solvent was left to evaporate at room temperature. After solvent evaporation, the scaffolds were washed thoroughly with distillate water during 3 days until complete salt removal. The scaffold was then extracted from the petri dish and dried at room temperature (Figure 4).

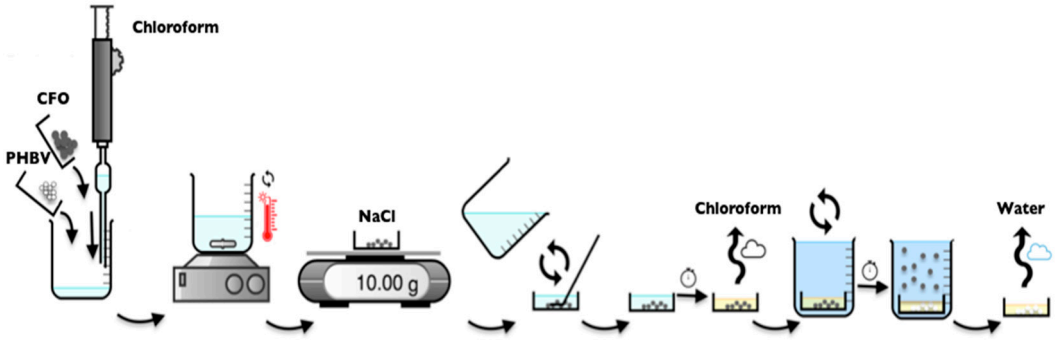

Figure 4 - Schematic representation of the preparation procedure of the PHBV scaffolds.

Table 1 summarizes the different procedures for the processing of PHBV and PHBV/CFO composites into different morphologies, as well as the corresponding nomenclature.

Table 1 - Procedures for the processing of PHBV and PHBV/CFO composites into different morphologies.

Nomenclature	Composition	Morphology	Processing technique
Film	PHBV	Film	Solvent-casting
Film CFO	PHBV, $CoFe_2O_4$		
Fibres R	PHBV	Randomly oriented fibres	Electrospinning
Fibres R CFO	PHBV, $CoFe_2O_4$		
Fibres O	PHBV	Oriented fibres	
Fibres O CFO	PHBV, $CoFe_2O_4$		
Microspheres	PHBV	Microspheres	Oil/Water emulsion
Microspheres CFO	PHBV, $CoFe_2O_4$		
Scaffold	PHBV	3D Scaffold	Solvent-casting/ Particulate leaching
Scaffold CFO	PHBV, $CoFe_2O_4$		

Preprints (www.preprints.org) | NOT PEER-REVIEWED | Posted: 3 July 2018 doi:10.20944/preprints201807.0021.v1

Peer-reviewed version available at Int. J. Mol. Sci. 2018, 19, 2149; doi:10.3390/ijms19082149

2.4. Characterization

The morphology of the PHBV and PHBV composites processed by the different methods was analyzed by scanning electron microscopy (SEM) with a FEG-SEM Hitachi with a 3 kV beam acceleration. The analyzed samples were previously coated with a thin gold layer using a sputtering coating (Polaron, model SC502). The size of the prepared microspheres, fibres and the pore size of the scaffolds were examined by ImageJ software.

Infrared measurements (FTIR) were performed in a Jasco FT/IR 4100 apparatus in ATR mode from 4000 to 600 cm^{-1}. FTIR spectra were collected after 64 scans with a resolution of 4 cm^{-1}.

Differential scanning calorimetry (DSC) measurements were performed in a Mettler Toledo DSC822e apparatus using a heating rate of 10 ºC.min^{-1} under a nitrogen purge (50 mL.min^{-1}). The samples were cut into small pieces from the middle region of the films and placed into 40 µL aluminum pans.

Thermogravimetry analyses were performed with a thermal analyzer TGA/SDTA 851e from Mettler Toledo. The samples were heated between 25 and 900 ºC, at a heating rate of 10 ºC.min^{-1} under a nitrogen flow rate of 50 mL.min^{-1}.

Mechanical measurements were performed on the different samples in a Shimadzu AG-IS universal testing machine at a test velocity of 1 mm.min^{-1} and room temperature. For the PHBV films and fibres, rectangular samples (25 x 10 mm) with thickness between 2-30 µm (Fischer Dualscope 603-478, digital micrometer) were cut and the mechanical measurements were performed in the tensile mode with a loading cell of 50 N. For the PHBV scaffold, cylindrical samples with approximately 6 mm diameter and 3.5 mm height were cut and the mechanical measurements were performed in the compression mode with a loading cell of 500 N. The scaffolds were submitted to a compressive-strain cycle load up to 20 cycles at a strain of 10%. The mechanical parameters were calculated from the average of triplicate measurements. The modulus of elasticity (*E*) was determined in the linear zone of elasticity, between 0% and 1% strain, using Hooke's law, obtaining the effective Young's modulus of the PHBV samples.

Contact angle measurements were performed at room temperature in a Data Physics OCA20 device using ultra-pure water as drop test liquid. The water drops (3 µL) were deposited on the sample surface and analyzed with SCA20 software. At least six

Preprints (www.preprints.org) | NOT PEER-REVIEWED | Posted: 3 July 2018 doi:10.20944/preprints201807.0021.v1

Peer-reviewed version available at Int. J. Mol. Sci. 2018, 19, 2149; doi:10.3390/ijms19082149

measurements in each sample were carried out at different sample locations and the average contact angle was taken as the result for each sample.

The magnetic behavior of the composite samples was evaluated at room temperature using a MicroSense EZ7-VSM vibrating sample magnetometer (VSM) from −18000 Oe to 18000 Oe.

2.5. Cytotoxicity assay

Indirect cytotoxicity assays were carried out to test if the samples present cytotoxic effect. This assay was adapted from ISO 10993-5 [5] and the cell viability estimated through 3-(4,5-dimethylthiazol-2-yl)-2,5-diphenyltetrazolium bromide (MTT) assay.

Polymer and composite samples were cut into 13 mm diameter discs. These samples were sterilized by the exposition to ultraviolet (UV) light for 1 h each side and washed 5 times in a phosphate buffer saline (PBS) solution for 5 min. After that, the different samples were put into 24-well plates, covered with 500 µL of Dulbecco's Modified Eagles' Medium (DMEM, Gibco) containing 1 $g.L^{-1}$ glucose supplemented with 10% Fetal Bovine Serum (FBS, Biochrom) and 1% Penicillin/Streptomycin (P/S, Biochrom). Pre-osteoblastic cells, MC3T3-E1, were seeded at $2x10^4$ $cells.mL^{-1}$ (cultured with the same DMEM) on 96 well plates and placed on a 5% CO_2 controlled atmosphere with 95% humidity at 37 ºC for 24 h. Then, the medium was removed from the 96-well plate and replaced by 100 µl of medium previously in contact with the polymer/composite samples. After medium replacement, the 96-well plate was placed for an additional 72 h on standardized culture conditions as mentioned above. A solution of 20% Dimethyl sulfoxide (DMSO) was used for positive control. After this incubation time, the cultured medium was again replaced by a 10% MTT solution on DMEM. After incubation for 2 h, MTT crystal were dissolved in DMSO and read at 570 nm on a spectrofluorimeter. Cell viability was calculated according to equation 1 [5].

$$Cell\ viability\ (\%) = \frac{Sample\ absorbance}{Positive\ control\ absorbance} x100 \qquad \text{(Equation 1)}$$

Peer-reviewed version available at Int. J. Mol. Sci. 2018, 19, 2149; doi:10.3390/ijms19082149

3. Results and discussion

3.1. Morphological characterization

PHBV and PHBV/CFO composites were processed into different morphologies by different methods in order to obtain a wide range of morphologies suitable for tissue engineering applications. The morphology of the samples, obtained by SEM images, is presented in Figure 5.

Figure 5 shows that both PHBV and PHBV/CFO composites can be successfully processed into different morphologies such as films, random and aligned fibres, microspheres and scaffolds. The insets show the diameter distribution of fibres, microspheres and the pore size of the porous scaffolds.

The presence of CFO nanoparticles is observed in the composite films (Figure 5b). The introduction of CFO nanoparticles does not promote changes in the average thickness of the films ($\approx 32 \pm 0.9$ µm). Random and aligned fibres with the absence of beads and with an average diameter of 4.4 ± 0.6 µm and 1.7 ± 0.2 µm, respectively, were obtained by electrospinning (Figure 5c and 5d, respectively). Similar to the films, no significant differences were observed in the morphology of the fibres before and after CFO nanoparticle incorporation (Figure 5c-f).

The histograms of Figure 5 show that the highest average fibre diameter is observed for randomly oriented fibres with and without CFO nanoparticles. For the oriented fibers, a lower average fiber diameter is observed because the rotating collector promotes the stretching of the deposited fibers on the collector, originating thinner fibres. It is noteworthy that the inclusion of CFO nanoparticles does not promote changes in the surface morphology of the fibres or in their average fibre diameter, being the average diameter of the randomly oriented and oriented fibres 4.4 ± 0.7 and 1.4 ± 0.5µm, respectively.

Neat and magnetic microspheres with a smooth surface and an average diameter ranging between 0.8 ± 0.2 µm (Figure 5g and 5h) were obtained by an oil-in-water emulsion procedure. Again, no significant differences in microsphere diameter were observed when 10 wt.% of CFO nanoparticles were introduced in the spheres.

Figure 5i and 5j show that PHBV and PHBV/CFO porous scaffolds can be obtained by the salt leaching method with NaCl crystals as a sacrificial material. A highly porous microstructure is observed with the presence of pores in the same range of the sacrificial material (262-370 µm) [28].

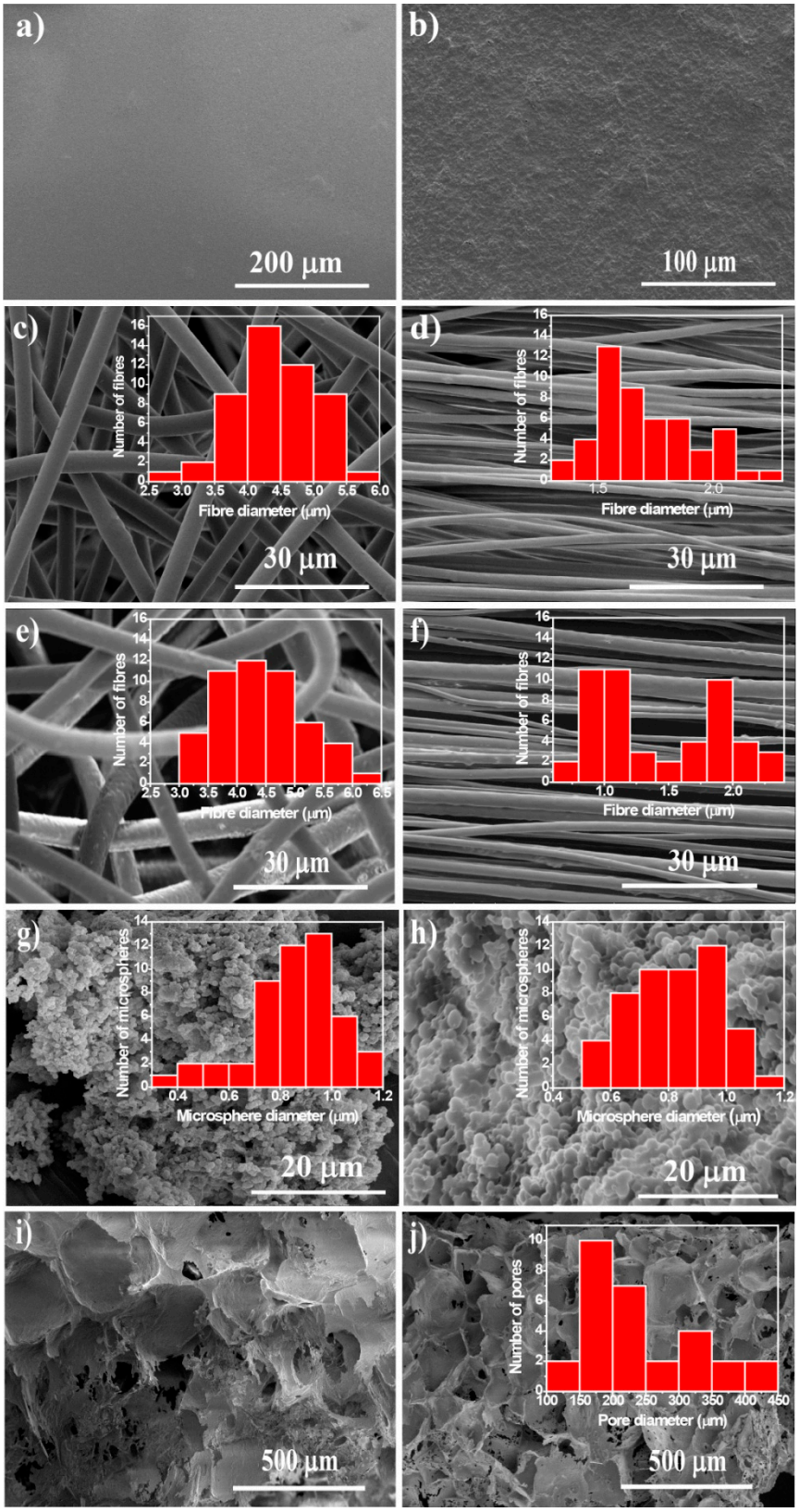

Figure 5. PHBV morphologies: a) neat PHBV films, b) CFO films, c) R fibres, d) O fibres e) R CFO fibres, f) O CFO fibres, g) neat PHBV microspheres, h) CFO

microspheres, i) scaffolds, j) CFO scaffolds. The histograms with the corresponding fibre, sphere and pore diameters are presented as figure inset.

3.2. Physico-chemical properties

To evaluate possible physicochemical modifications in the properties of PHBV after the different processing conditions and the inclusion of the CFO nanoparticles, FTIR-ATR, DSC and TGA measurements were performed.

Figure 6a shows the FTIR spectra of neat PHBV processed into the different morphologies. The main characteristic absorption bands of PHBV are observed, namely the absorption bands in the region of 826-979 cm^{-1} and the region of 1227-1478 cm^{-1}, which are related to C-H stretching. The absorption bands at 1057, 1133 and 1183 cm^{-1} are assigned to the C-O stretching [29-30] and the absorption band at approximately 1720 cm^{-1} is associated to the C=O vibrational mode [29-30]. No variations are observed, independently of the different processing conditions and morphologies.

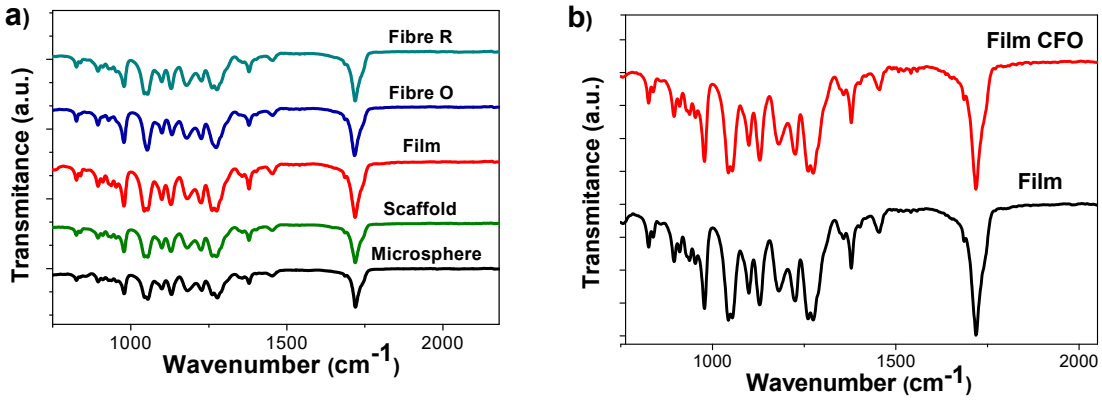

Figure 6. FTIR-ATR spectra of the a) neat PHBV processing into different morphologies and b) PHBV/CFO film composites.

The FTIR-ATR measurements were also performed for the different morphologies with CFO nanoparticles to evaluate the influence of the inclusion of the nanoparticles in the chemical structure of PHBV. As a representative example, Figure 6b shows the FTIR spectra obtained for neat and PHBV composite films. It is worth to mention that no differences were observed in the absorption bands of PHBV after the inclusion of the CFO nanoparticles, indicating that the CFO nanoparticles do not present strong interaction with polymer chemical structure. Similar results were obtained for the fibres, microspheres, and scaffolds.

Preprints (www.preprints.org) | NOT PEER-REVIEWED | Posted: 3 July 2018 doi:10.20944/preprints201807.0021.v1

Peer-reviewed version available at Int. J. Mol. Sci. 2018, 19, 2149; doi:10.3390/ijms19082149

3.3. Thermal analysis

The thermal characterization of neat PHBV and PHBV/CFO composites was performed by DSC and TGA analysis.

Figure 7a shows the DSC thermograms of the different PHBV morphologies and PHBV/CFO composite films. The melting temperature and the enthalpy associated to each endothermic peak is presented in table 2. All samples exhibit an intense endothermic peak between 160 and 180 ºC corresponding to the melting peak of PHBV [31]. The inclusion of CFO nanoparticles does not induce relevant modification to this behavior (Figure 7b), the composite films showing a broad peak corresponding to the melting temperature between 160-180 ºC. Similar results were obtained for other PHBV composites.

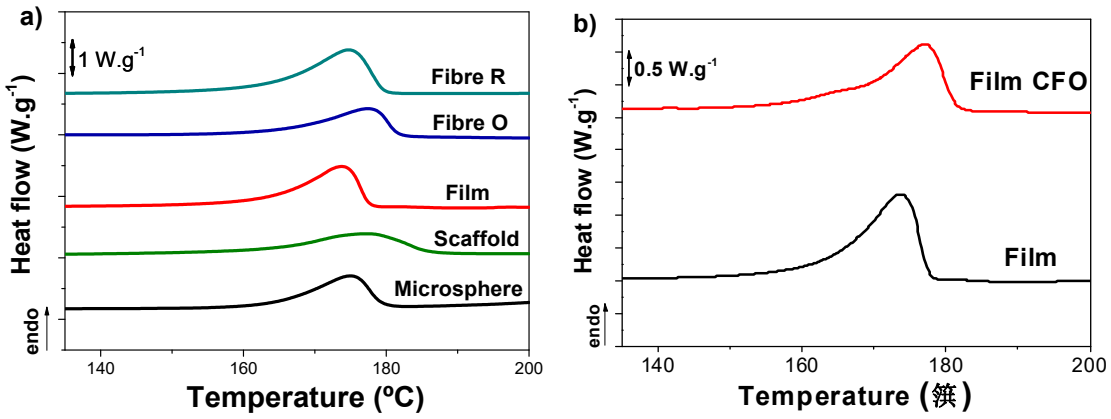

Figure 7. DSC thermograms for a) different neat PHBV morphologies and b) PHBV films and films composites.

From the enthalpy of the melting peak, the degree of crystallinity (X_C) of neat PHBV morphologies and PHBV composites was obtained, by applying equation 2.

$$X_c = \frac{\Delta H_m}{\Delta H_{mo}} \qquad \textbf{(Equation 2)}$$

where ΔH_m is the area of the melting peak and ΔH_{m0} the enthalpy of 100% PHBV crystalline (146.6 J.mol^{-1}) [32].

The degree of crystallinity of the different samples is presented in table 2. All samples show degrees of crystallinity between 40 and 67%, being the largest degree of crystallinity is those of the films and the randomly oriented fibers (above 50%) and lower for the rest of the samples (40 and 50%). These variations in the degree of

Preprints (www.preprints.org) | NOT PEER-REVIEWED | Posted: 3 July 2018 doi:10.20944/preprints201807.0021.v1

Peer-reviewed version available at Int. J. Mol. Sci. 2018, 19, 2149; doi:10.3390/ijms19082149

crystallinity are related with the different crystallizations conditions corresponding to the different processing conditions and morphologies, and have been specifically explored in the literature for related systems [17] for fibre [33-34], sphere [26], scaffold [35-36] and film [37-38] morphologies. The inclusion of CFO nanoparticles induces a decrease of the degree of crystallinity for films and for random fibres, which indicates the CFO nanoparticles act as defects during the crystallization process [39], hindering also spherulite growth [40]. Interestingly, the same behavior is not observed for aligned fibres, where a slight increase is observed (~9%), contrary to the observed in the literature with different polymers [27,39], which can be ascribed to the polymer stretching and acceleration during the jet formation. The increase in the crystallinity degree observed for oriented fibres composites can be attributed to variations in the stretching of the jet during the electrospinning process, due to the modifications of the viscosity and electrical characteristics of the solution.

Table 2. T_m, ΔH_m, and crystallinity degree of all PHB and PHBV composite samples. The associated error is ± 2%.

Sample	T_m (°C)	ΔH_m (J.g^{-1})	X_c (%)
Film	174	82	56
Film/CFO	177	70	48
R fibres	175	98	67
R/CFO fibres	177	67	46
O fibres	177	65	45
O/CFO fibres	179	79	54
Microsphere	175	57	39
Microsphere/CFO	174	57	39
Scaffold	177	63	43
Scaffold/CFO	182	61	42

TGA was performed to determining the thermal stability of the different PHBV morphologies and that of the corresponding composites with 10%wt of CFO. Figure 8 shows the TGA curves of the different PHBV samples as well as the corresponding first derivatives. The different PHBV morphologies without CFO degraded with negligible

Preprints (www.preprints.org) | NOT PEER-REVIEWED | Posted: 3 July 2018 doi:10.20944/preprints201807.0021.v1

Peer-reviewed version available at Int. J. Mol. Sci. 2018, 19, 2149; doi:10.3390/ijms19082149

residue, whereas the composite samples leave a residue of approximately 10% that is related to the CFO content.

Thermal degradation of the different samples occurs in one weight loss step, the onset and peak degradation temperature depending on the processed morphology. Comparing the degradation temperature of the different PHBV morphologies (Figure 8a), it is observed that the scaffold (degradation peak = 290º) is thermally less stable than the rest of the samples, with a degradation peak around 300º. This difference should be attributed to the interaction of the polymer chains with the salt during the preparation process and polymer crystallization, leading to a less stable polymer.

With respect to the polymer composites, the onset and peak degradation temperature of the PHBV films with CFO is shifted towards lower temperatures. The same is observed for the others composites (data not shown). Thus, the higher thermal conductivity of the nanoparticles with respect to the polymer matrix, lead to an earlier degradation process. Regarding to this, contradictory results can be found in literature. Thus, it has been reported that the introduction of CFO in a PVDF polymer matrix, leads to an increase of the thermal stability [41], as well as the introduction of silver nanoparticles in PHBV [42]. Contrary, the introduction of organophilic attapulgite (MAT) in PHBV [43] and magnetite in chitosan derivatives [44] leads to a decrease in the thermal stability of the nanocomposites.

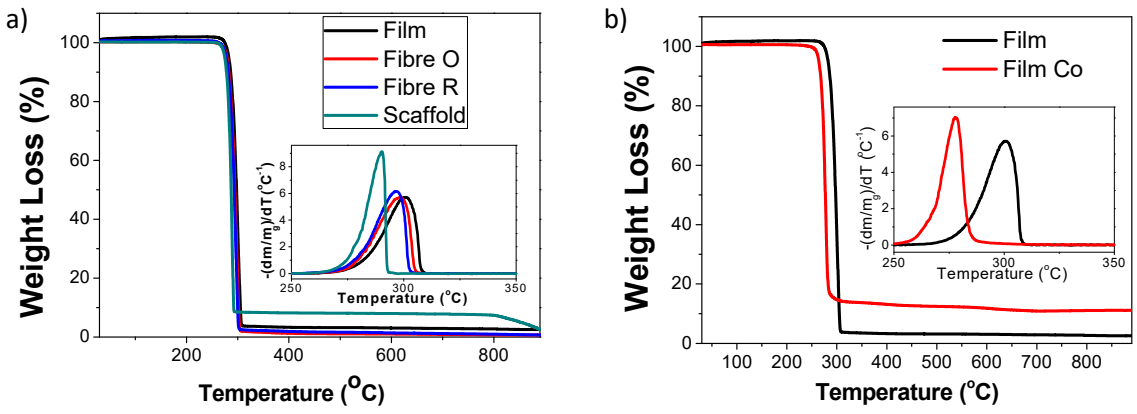

Figure 8. TGA thermograms and corresponding first derivatives for a) different neat PHBV morphologies and b) PHBV films and films composites.

Preprints (www.preprints.org) | NOT PEER-REVIEWED | Posted: 3 July 2018 doi:10.20944/preprints201807.0021.v1

Peer-reviewed version available at Int. J. Mol. Sci. 2018, 19, 2149; doi:10.3390/ijms19082149

3.4. Magnetic properties of the composites

The quantification of the magnetic nanoparticle content of the composites was assessed by VSM. Figure 9 shows the magnetization curves of the different PHBV composites determined at room temperature. The inset in Figure 9 represents the magnetization curve of CFO in the form of nanopowder. The CFO nanoparticles reveal an hysteresis loop with coercivity at 24 emu.g^{-1} and a maximum magnetization of 43 emu.g^{-1}, at approximately 5000 Oe applied magnetic field [39].

As for CFO nanopowders, the magnetization of the composites increases with increasing magnetic field until saturation, reaching a maximum saturation at approximately 20000 Oe. By comparing the maximum magnetization saturation of the CFO/PHBV composites it is observed that it is higher for the PHBV/CFO films (6.2 emu.g^{-1}), followed by the scaffolds (Figure 9), which was attributed to the different nanofiller content, i.e. some fillers were not integrated in the samples, depending on the processing conditions and sample morphology.

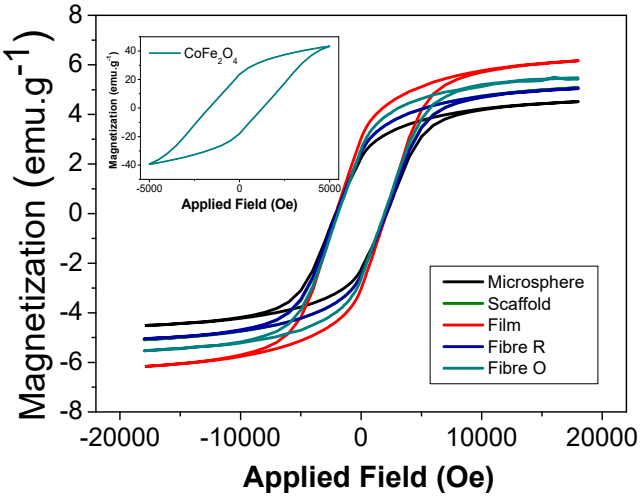

Figure 9. Room temperature hysteresis curves for the CFO/PHBV composites.

3.3. Contact angle measurements

Wettability was also assessed for the different samples through sessile drop technique. The results are present in the table 4.

Table 4 - Water contact angle measurement for the different samples (mean ± SD).

Film	Film CFO	Fibres O	Fibres O CFO	Fibres R	Fibres R CFO	Scaffold	Scaffold CFO
90 ± 12º	96 ± 4º	103 ± 11º	119 ± 5º	125 ± 2º	128 ± 2º	97 ± 13º	106 ± 9º

Preprints (www.preprints.org) | NOT PEER-REVIEWED | Posted: 3 July 2018 doi:10.20944/preprints201807.0021.v1

Peer-reviewed version available at Int. J. Mol. Sci. 2018, 19, 2149; doi:10.3390/ijms19082149

All samples show contact angles above 90º, presenting an hydrophobic behaviour [45]. Fibres show higher contact angles reaching 128 ± 2º while films show the lowest, 90 ± 12º. Differences in wettability between samples are attributed to their morphological differences, which lead to different submicron roughness. For example, the electrospinning technique generates roughness in the sub-micron range since both fibrils and fibre separation are in this order of magnitude [46].

Moreover, the introduction of cobalt ferrite particles leads to an increase of the contact angle of all the morphologies. This increase is associated to the increase of the surface roughness that is related to the introduction of the particles in the polymer [47].

3.4. Mechanical properties

The influence of the morphology on the mechanical response was evaluated by stress-strain mechanical measurements for the films and fibres and compression for the scaffolds (Figure 10). The corresponding Young modulus is presented in Table 5.

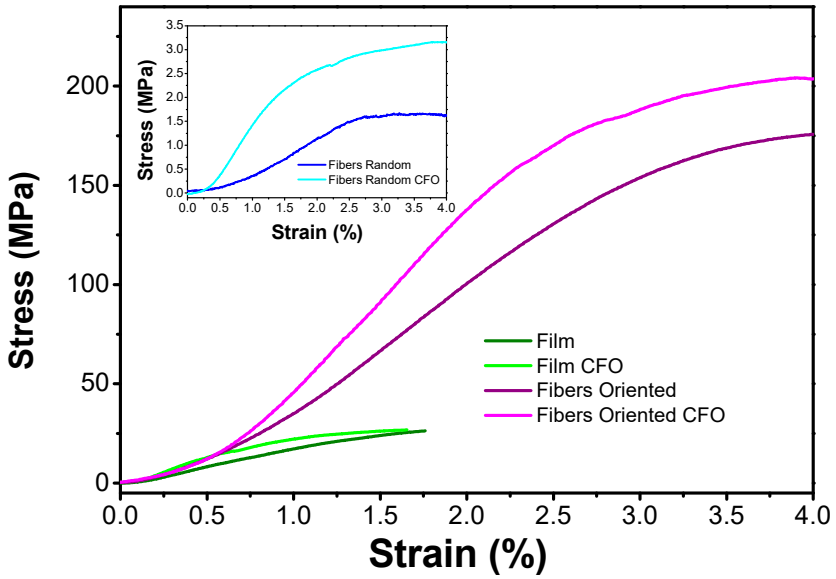

Figure 10. Mechanical stress-strain behavior of the different PHBV samples with and without CFO.

Comparing the Young's modulus of the different morphologies, it is verified that the fibres present higher values and the scaffolds the lower. Comparing random and oriented fibres, the lower values of Young's modulus are explained by the fact that when

the fibers are stretched, they are reoriented along the stretching axis with low effective Young's Modulus, contrary to the oriented fibers that are already aligned long the stretching axis during processing and therefore the response of the material and not the reorientation of the matt is measured. Regarding the incorporation of CFO in the polymer matrix, previous study shown that the incorporation of CFO in fibre mats increase their Young's modulus [27] due to the electrostatic interaction between fillers and polymer chains and the proper wetting of the fillers by the polymer. This is in agreement with the presented results, where the introduction of particles leads to an increase of this value in all the morphologies.

Table 5 - Young modulus of the different PHBV samples. Values shown as mean ± SD.

Morphologies	E (MPa)
Film	17 ± 5
Film CFO	27 ± 5
Fibres R	1.1 ± 0.6
Fibres R CFO	1.7 ± 0,5
Fibres O	66 ± 41
Fibres O CFO	83 ± 9
Scaffold	$8.9 \times 10^{-3} \pm 1.7 \times 10^{-3}$
Scaffold CFO	$1.3 \times 10^{-2} \pm 6.4 \times 10^{-4}$

In relation to the PHBV scaffolds, compression cycles were performed in order to mimic the constant compressions to which the scaffold is subjected during *in vivo* or *in vitro* applications. The characteristics stress–strain curve of the PHBV scaffolds with CFO for compression assays at 10% along the different number of cycles is presented in the Figure 11b. The Young modulus of the PHBV scaffolds with and without CFO along the compression cycles is presented in Figure 11. It is observed that the Young's Modulus decreases from the first to the second cycle, being more pronounced in the scaffolds with CFO. After that, this value stabilizes and keeps relatively constant up to the 20th cycle. The incorporation of CFO in the PHBV scaffold leads first to an increase of the Young modulus value, however, with the increase of the number of compression cycles, this value becomes lower than that of the PHBV scaffold. The addition of CFO leads to some mechanical instability observed by the more pronounced drop in Young's Modulus in the first cycles. Comparing to PVDF scaffolds prepared by the same

Preprints (www.preprints.org) | NOT PEER-REVIEWED | Posted: 3 July 2018 doi:10.20944/preprints201807.0021.v1

Peer-reviewed version available at Int. J. Mol. Sci. 2018, 19, 2149; doi:10.3390/ijms19082149

technique, the PHBV scaffolds achieved slightly smaller Young Modulus values and both polymers exhibited a drop as cycles progressed [28].

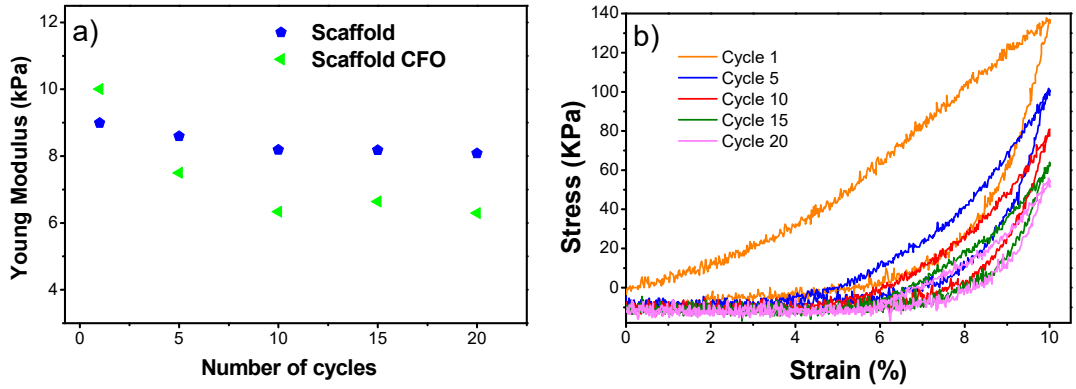

Figure 11. a)Young modulus of the PHBV scaffolds with and without CFO along the compression cycles and b) Characteristics stress–strain curves of the PHBV scaffolds with CFO for compression assays at 10%.

3.5. Cytotoxicity evaluation

The results of the effect of the extract of the different samples on cell viability are presented in Figure 12. It is verified that all the samples do not show any cytotoxic effect (cell viability values higher than 70%). Regarding the samples with CFO in the polymer matrix, it is thus deduced that the particles are efficiently encapsulated, once these particles are cytotoxicity [20,21]. In this way, these samples can be used for biomedical applications, and more particularly for tissue engineering applications.

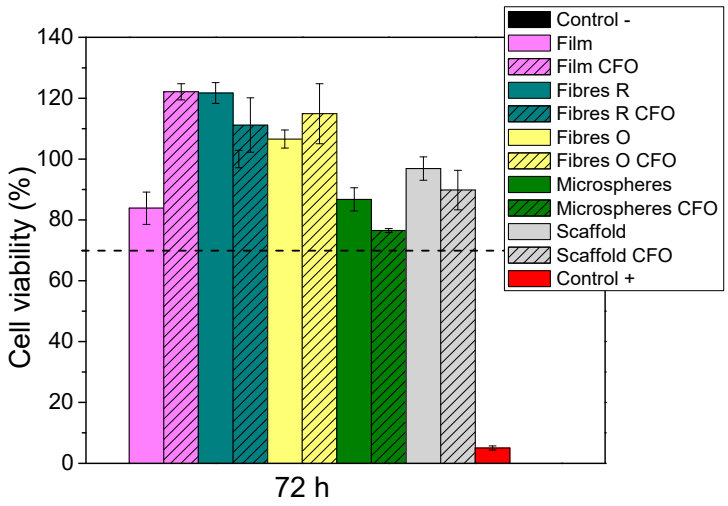

Peer-reviewed version available at Int. J. Mol. Sci. 2018, 19, 2149; doi:10.3390/ijms19082149

Figure 12 - Cytotoxicity assay of MC3T3-E1 pre-osteoblast cells in contact with the as-prepared extraction media exposed to the different PHBV samples for 72 h (relative cell viability was presented as the percentage of the negative control (n = 4 ± SD).

4. Conclusions

Different PHBV morphologies - film, fibres, microspheres and scaffolds - with and without CFO were successfully obtained. The physico-chemical, thermal, magnetic and mechanical properties of the PHBV pristine and composites samples were evaluated. All the samples produced present a hydrophobic behaviour. It is verified that the introduction of cobalt ferrites induces changes in the degree of crystallinity: a decrease in the film (≈ 8%) and randomly oriented fibres (≈ 21%) and an increase in the aligned fibres (≈ 9%). Relatively to the thermal degradation, it was observed that the scaffold is thermally less stable than the others morphologies and that the CFO introduction leads to an increase of the thermal stability. The mechanical properties depend on the morphology (the fibres present higher values and the scaffolds the lower) and the addition of cobalt ferrites improves this value, being more pronounced in the aligned fibres. Their cytotoxic behaviour was also evaluated and it was verified that all the produced samples are no cytotoxic, indicating their suitability for tissue engineering applications.

Acknowledgments

The authors thank the FCT (Fundação para a Ciência e Tecnologia) for financial support under framework of the Strategic Funding UID/FIS/04650/2013, UID/QUI/00686/2013 and UID/QUI/0686/2016 and project PTDC/EEI-SII/5582/2014 and project POCI-01-0145-FEDER-028237. Funds provided by FCT in the framework of EuroNanoMed 2016 call, Project LungChek ENMed/0049/2016 are also gratefully acknowledged. DMC and CR also thank the FCT for the grants SFRH/BPD/121526/2016 and SFRH/BPD/90870/2012, respectively. Finally, the authors acknowledge funding by the Spanish Ministry of Economy and Competitiveness (MINECO) through the project MAT2016-76039-C4-3-R (AEI/FEDER, UE) and from the Basque Government Industry Department under the ELKARTEK and HAZITEK program.

References

1. Ma, P.X. Biomimetic materials for tissue engineering. *Adv Drug Deliver Rev* **2008**, *60*, 184-198.
2. Shin, H.; Jo, S.; Mikos, A.G. Biomimetic materials for tissue engineering. *Biomaterials* **2003**, *24*, 4353-4364.
3. Howard, D.; Buttery, L.D.; Shakesheff, K.M.; Roberts, S.J. Tissue engineering: Strategies, stem cells and scaffolds. *J Anat* **2008**, *213*, 66-72.
4. Rezwan, K.; Chen, Q.Z.; Blaker, J.J.; Boccaccini, A.R. Biodegradable and bioactive porous polymer/inorganic composite scaffolds for bone tissue engineering. *Biomaterials* **2006**, *27*, 3413-3431.
5. O'Brien, F.J. Biomaterials & scaffolds for tissue engineering. *Mater Today* **2011**, *14*, 88-95.
6. Rahman, M.S.; Tsuchiya, T. Enhancement of chondrogenic differentiation of human articular chondrocytes by biodegradable polymers. *Tissue Eng* **2001**, *7*, 781-790.
7. Parssinen, J.; Hammaren, H.; Rahikainen, R.; Sencadas, V.; Ribeiro, C.; Vanhatupa, S.; Miettinen, S.; Lanceros-Mendez, S.; Hytonen, V.P. Enhancement of adhesion and promotion of osteogenic differentiation of human adipose stem cells by poled electroactive poly(vinylidene fluoride). *J Biomed Mater Res A* **2015**, *103*, 919-928.
8. Doyle, C.; Tanner, E.T.; Bonfield, W. In vitro and in vivo evaluation of polyhydroxybutyrate and of polyhydroxybutyrate reinforced with hydroxyapatite. *Biomaterials* **1991**, *12*, 841-847.
9. Kose, G.T.; Korkusuz, F.; Korkusuz, P.; Hasirci, V. In vivo tissue engineering of bone using poly(3-hydroxybutyric acid-co-3-hydroxyvaleric acid) and collagen scaffolds. *Tissue Eng* **2004**, *10*, 1234-1250.
10. Fukada, E.; Ando, Y. Piezoelectric properties of poly-β-hydroxybutyrate and copolymers of β-hydroxybutyrate and β-hydroxyvalerate. *International journal of biological macromolecules* **1986**, *8*, 361-366.
11. Ohigashi, H. Piezoelectric polymers–materials and manufacture. *Japanese Journal of Applied Physics* **1985**, *24*, 23.
12. Ando, M.; Kawamura, H.; Kageyama, K.; Tajitsu, Y. Film sensor device fabricated by a piezoelectric poly(l-lactic acid) film. *Japanese Journal of Applied Physics* **2012**, *51*.
13. Ribeiro, C.; Moreira, S.; Correia, V.; Sencadas, V.; Rocha, J.G.; Gama, F.M.; Ribelles, J.L.G.; Lanceros-Mendez, S. Enhanced proliferation of pre-osteoblastic cells by dynamic piezoelectric stimulation. *Rsc Adv* **2012**, *2*, 11504-11509.
14. Martins, P.M.; Ribeiro, S.; Ribeiro, C.; Sencadas, V.; Gomes, A.C.; Gama, F.M.; Lanceros-Mendez, S. Effect of poling state and morphology of piezoelectric poly(vinylidene fluoride) membranes for skeletal muscle tissue engineering. *Rsc Adv* **2013**, *3*, 17938-17944.
15. Ribeiro, C.; Sencadas, V.; Correia, D.M.; Lanceros-Mendez, S. Piezoelectric polymers as biomaterials for tissue engineering applications. *Colloids and Surfaces B-Biointerfaces* **2015**, *136*, 46-55.
16. Chen, G.Q.; Wu, Q. The application of polyhydroxyalkanoates as tissue engineering materials. *Biomaterials* **2005**, *26*, 6565-6578.
17. Ribeiro, C.; Costa, C.M.; Correia, D.M.; Nunes-Pereira, J.; Oliveira, J.; Martins, P.; Gonçalves, R.; Cardoso, V.F.; Lanceros-Méndez, S. Electroactive poly(vinylidene fluoride)-based structures for advanced applications. *Nature Protocols* **2018**, *13*, 681-704.
18. Ribeiro, C.; Correia, V.; Martins, P.; Gama, F.M.; Lanceros-Mendez, S. Proving the suitability of magnetoelectric stimuli for tissue engineering applications. *Colloids and Surfaces B: Biointerfaces* **2016**, *140*, 430-436.

19. Martins, P.; Lanceros-Mendez, S. Polymer-based magnetoelectric materials. *Adv Funct Mater* **2013**, *23*, 3371-3385.
20. Cho, K.H.; Bichurin, M.I.; Petrov, V.M.; Bhalla, A.; Priya, S. Magnetoelectric laminate composite: Effect of piezoelectric layer on magnetoelectric properties. *Ferroelectrics* **2014**, *473*, 110-128.
21. Wickens, A.; Robinson, J. Magnetoelectric neural modulation. *Biophys J* **2017**, *112*, 286a-286a.
22. Ribeiro, C.; Correia, D.; Ribeiro, S.; Fernandes, M.; Lanceros-Mendez, S. Piezo-and magnetoelectric polymers as biomaterials for novel tissue engineering strategies. *MRS Advances* **2018**, 1-6.
23. Ribeiro, C.; Correia, V.; Martins, P.; Gama, F.M.; Lanceros-Mendez, S. Proving the suitability of magnetoelectric stimuli for tissue engineering applications. *Colloid Surface B* **2016**, *140*, 430-436.
24. Hu, J.M.; Nan, T.X.; Sun, N.X.; Chen, L.Q. Multiferroic magnetoelectric nanostructures for novel device applications. *Mrs Bull* **2015**, *40*, 728-735.
25. Martins, P.; Gonçalves, R.; Lanceros-Mendez, S.; Lasheras, A.; Gutiérrez, J.; Barandiarán, J.M. Effect of filler dispersion and dispersion method on the piezoelectric and magnetoelectric response of cofe2o4/p(vdf-trfe) nanocomposites. *Applied Surface Science* **2014**, *313*, 215-219.
26. Correia, D.M.; Sencadas, V.; Ribeiro, C.; Martins, P.M.; Martins, P.; Gama, F.M.; Botelho, G.; Lanceros-Méndez, S. Processing and size range separation of pristine and magnetic poly(l-lactic acid) based microspheres for biomedical applications. *Journal of Colloid and Interface Science* **2016**, *476*, 79-86.
27. Maciel, M.M.; Ribeiro, S.; Ribeiro, C.; Francesko, A.; Maceiras, A.; Vilas, J.L.; Lanceros-Méndez, S. Relation between fiber orientation and mechanical properties of nano-engineered poly(vinylidene fluoride) electrospun composite fiber mats. *Composites Part B: Engineering* **2018**, *139*, 146-154.
28. Correia, D.M.; Ribeiro, C.; Sencadas, V.; Vikingsson, L.; Oliver Gasch, M.; Gómez Ribelles, J.L.; Botelho, G.; Lanceros-Méndez, S. Strategies for the development of three dimensional scaffolds from piezoelectric poly(vinylidene fluoride). *Materials & Design* **2016**, *92*, 674-681.
29. Fei, B.; Chen, C.; Wu, H.; Peng, S.; Wang, X.; Dong, L. Quantitative ftir study of phbv/bisphenol a blends. *European Polymer Journal* **2003**, *39*, 1939-1946.
30. Kim, G.M.; Michler, G.H.; Henning, S.; Radusch, H.J.; Wutzler, A. Thermal and spectroscopic characterization of microbial poly(3-hydroxybutyrate) submicrometer fibers prepared by electrospinning. *Journal of Applied Polymer Science* **2007**, *103*, 1860-1867.
31. Xu, Y.; Zou, L.; Lu, H.; Wei, Y.; Hua, J.; Chen, S. Preparation and characterization of electrospun phbv/peo mats: The role of solvent and peo component. *Journal of Materials Science* **2016**, *51*, 5695-5711.
32. Yu, H.-y.; Qin, Z.-y.; Zhou, Z. Cellulose nanocrystals as green fillers to improve crystallization and hydrophilic property of poly(3-hydroxybutyrate-co-3-hydroxyvalerate). *Progress in Natural Science: Materials International* **2011**, *21*, 478-484.
33. Ribeiro, C.; Moreira, S.; Correia, V.; Sencadas, V.; Rocha, J.G.; Gama, F.M.; Gomez Ribelles, J.L.; Lanceros-Mendez, S. Enhanced proliferation of pre-osteoblastic cells by dynamic piezoelectric stimulation. *RSC Advances* **2012**, *2*, 11504-11509.
34. Ribeiro, C.; Pärssinen, J.; Sencadas, V.; Correia, V.; Miettinen, S.; Hytönen Vesa, P.; Lanceros-Méndez, S. Dynamic piezoelectric stimulation enhances osteogenic differentiation of human adipose stem cells. *Journal of Biomedical Materials Research Part A* **2014**, *103*, 2172-2175.

35. Correia, D.M.; Ribeiro, C.; Sencadas, V.; Vikingsson, L.; Oliver Gasch, M.; Gómez Ribelles, J.L.; Botelho, G.; Lanceros-Méndez, S. Strategies for the development of three dimensional scaffolds from piezoelectric poly(vinylidene fluoride). *Materials and Design* **2016**, *92*, 674-681.
36. Khorasani, M.T.; Mirmohammadi, S.A.; Irani, S. Polyhydroxybutyrate (phb) scaffolds as a model for nerve tissue engineering application: Fabrication and in vitro assay. *International Journal of Polymeric Materials and Polymeric Biomaterials* **2011**, *60*, 562-575.
37. El-Hadi, A.; Schnabel, R.; Straube, E.; Müller, G.; Henning, S. Correlation between degree of crystallinity, morphology, glass temperature, mechanical properties and biodegradation of poly (3-hydroxyalkanoate) phas and their blends. *Polymer Testing* **2002**, *21*, 665-674.
38. Sencadas, V.; Gregorio Jr, R.; Lanceros-Méndez, S. A to β phase transformation and microestructural changes of pvdf films induced by uniaxial stretch. *Journal of Macromolecular Science, Part B: Physics* **2009**, *48*, 514-525.
39. Brito-Pereira, R.; Correia, D.M.; Ribeiro, C.; Francesko, A.; Etxebarria, I.; Pérez-Álvarez, L.; Vilas, J.L.; Martins, P.; Lanceros-Mendez, S. Silk fibroin-magnetic hybrid composite electrospun fibers for tissue engineering applications. *Composites Part B: Engineering* **2018**, *141*, 70-75.
40. Goncalves, R.; Martins, P.; Correia, D.M.; Sencadas, V.; Vilas, J.L.; Leon, L.M.; Botelho, G.; Lanceros-Mendez, S. Development of magnetoelectric cofe2o4 /poly(vinylidene fluoride) microspheres. *RSC Advances* **2015**, *5*, 35852-35857.
41. Martins, P.; Costa, C.M.; Benelmekki, M.; Botelho, G.; Lanceros-Mendez, S. On the origin of the electroactive poly(vinylidene fluoride) β-phase nucleation by ferrite nanoparticles via surface electrostatic interactions. *CrystEngComm* **2012**, *14*, 2807-2811.
42. Min, M.; Shi, Y.; Ma, H.; Huang, H.; Shi, J.; Chen, X.; Liu, Y.; Wang, L. Polymer-nanoparticle composites composed of poly(3-hydroxybutyrate-co-3-hydroxyvalerate) and coated silver nanoparticles. *Journal of Macromolecular Science, Part B* **2015**, *54*, 411-423.
43. Thiré, R.M.d.S.M.; Arruda, L.C.; Barreto, L.S. Morphology and thermal properties of poly(3-hydroxybutyrate-co-3-hydroxyvalerate)/attapulgite nanocomposites. *Materials Research* **2011**, *14*, 340-344.
44. Ziegler-Borowska, M.; Chełminiak, D.; Kaczmarek, H.; Kaczmarek-Kędziera, A. Effect of side substituents on thermal stability of the modified chitosan and its nanocomposites with magnetite. *Journal of Thermal Analysis and Calorimetry* **2016**, *124*, 1267-1280.
45. Yuan, Y.; Lee, T.R. Contact angle and wetting properties. In *Springer Series in Surface Sciences*, 2013; Vol. 51, pp 3-34.
46. Areias, A.C.; Ribeiro, C.; Sencadas, V.; Garcia-Giralt, N.; Diez-Perez, A.; Gómez Ribelles, J.L.; Lanceros-Méndez, S. Influence of crystallinity and fiber orientation on hydrophobicity and biological response of poly(l-lactide) electrospun mats. *Soft Matter* **2012**, *8*, 5818-5825.
47. Sun, T.; Feng, L.; Gao, X.; Jiang, L. Bioinspired surfaces with special wettability. *Accounts of Chemical Research* **2005**, *38*, 644-652.